Smart Structures and Systems, *Vol. 34, No. 1 (2024) 63-72*
https://doi.org/10.12989/sss.2024.34.1.063

Soil resistance estimation using smart instrumented dynamic penetrometers

Geunwoo Park [1a], Namsun Kim [1a], Yong-Hoon Byun [2b], Sang Yeob Kim [3c] and Jong-Sub Lee*[1]

[1] *School of Civil, Environmental and Architectural Engineering, Korea University, 145, Anam-ro, Seongbuk-gu, Seoul, 02841, Republic of Korea*
[2] *Department of Agricultural Civil Engineering, Kyungpook National University, 80, Daehak-ro, Buk-gu, Daegu, 41566, Republic of Korea*
[3] *Department of Fire and Disaster Prevention, Konkuk University, 268, Chungwon-daero, Chungju-si, Chungcheongbuk-do, 27478, Republic of Korea*

(*Received May 21, 2024, Revised August 21, 2024, Accepted August 21, 2024*)

Abstract. In-situ penetration tests using dynamic penetrometers are widely used for estimating soil resistance. Additionally, these dynamic penetrometers have been instrumented to improve tests accuracy. This paper introduces smart instrumented dynamic penetrometers and discusses experimental studies for various cases. An energy monitoring module was developed to enhance the dynamic penetration tests. The standard penetration test (SPT) and instrumented dynamic cone penetrometer (IDCP) tests were conducted using the energy monitoring module. Dynamic responses obtained by the energy monitoring module were used to calculate the transferred energies into the rod head and tip to correct the evaluation of ground strength. In addition, a crosshole-type dynamic penetrometer (CDP) was developed to measure the penetration index and shear wave velocity simultaneously to estimate the strength and stiffness of ground. The results of this study indicate that smart instrumented dynamic penetrometers may be effectively used to characterize the strength and stiffness of ground.

Keywords: Crosshole-type Dynamic Penetrometer (CDP); energy monitoring module; Instrumented Dynamic Cone Penetrometer (IDCP); Standard Penetration Test (SPT); Transferred energy

1. Introduction

Before the foundation design of structure, a dynamic penetration in-situ test should be conducted to characterize ground properties. Standard penetration test (SPT) is a representative dynamic penetration in-situ test. A constant potential energy of 473.5 N·m is applied to the SPT rod to penetrate the ground during the SPT. The number of blows for a 30 cm penetration depth is the SPT N-value after a 15 cm initial penetration depth. Engineering parameters such as elastic modulus, shear modulus, relative density, friction angle, and cohesion are estimated using relationships with the SPT N-value (Cubrinovski and Ishihara 1999, Anbazhagan *et al*. 2012, Kumar *et al*. 2016, Mujtaba *et al*. 2018). The ground is classified using the ranges of the SPT N-value. Furthermore, cone penetration test (CPT), which is static penetration in-situ test, is often conducted on the ground with the SPT. Corrected cone tip resistance (q_t) is measured and correlated with the SPT N-value (Arifuzzaman and Anisuzzaman 2022). In addition, the SPT N-value is used to evaluate the probability of liquefaction (Bolton Seed *et al*. 1985, Chang *et al*. 2011, Ji *et al*. 2021).

To improve the mobility and simplicity of dynamic penetration in-situ test, miniaturized dynamic penetrometers were developed. In 1956, Scala suggested the dynamic cone penetrometer (DCP). In 2009, the standard DCP test method was introduced in ASTM D6951. The standardized hammer weight and drop height are 78.5 N and 575 mm, respectively; thus, the potential energy is calculated to be 45.1 N·m. The apex angle and diameter of the DCP cone tip are 60° and 20 mm, respectively. During the DCP test, the penetration depth per a blow is recorded as the dynamic cone penetration index (DCPI). The DCPI is converted to several engineering parameters such as the elastic modulus, shear modulus, relative density, friction angle, California bearing ratio (CBR), and void ratio (Mohammadi *et al*. 2008, George *et al*. 2009, Sagar *et al*. 2022). Miniaturized dynamic penetrometers are effectively used for the characterization of low accessibility sites such as mountainous areas due to its high mobility. The DCP test is effectively used for slope stability assessment. The strength of slope is characterized based on the DCPI (Tsuchida *et al*. 2011, Sakib *et al*. 2022).

The SPT N-value and DCPI accuracy depend on the constant driving energy. However, inconsistent driving energy may be applied to the rod due to experimental conditions and energy losses caused by impedance mismatch and friction (Sjoblom *et al*. 2002). Furthermore, instrumented dynamic penetrometers were developed to energy correct the SPT N-value and DCPI. Dynamic responses at the SPT rod head were measured using a typical energy monitoring module to consider the device's

*Corresponding author, Ph.D., Professor,
E-mail: jongsub@korea.ac.kr
[a] Ph.D., Postdoctoral Researcher
[b] Ph.D., Associate Professor
[c] Ph.D., Assistant Professor

ISSN: 1738-1584 (Print), 1738-1991 (Online)

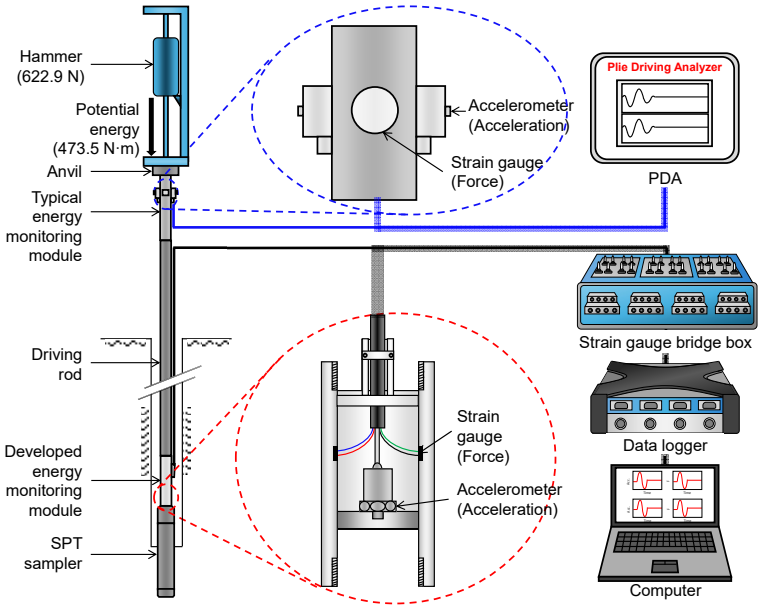

Fig. 1 Energy measurement system in SPT using energy monitoring modules

efficiency and energy loss at the anvil (Kovacs 1979). Transferred energy into the rod head is overestimated compared to actual penetration energy owing to the rod length effects and energy loss at joints (Lukiantchuki *et al*. 2011, Kim *et al*. 2022). An energy monitoring module for energy measurement at the SPT sampler was developed to calculate the transferred energy into the sampler (Hong *et al*. 2022). The transferred energy into the sampler is more similar to the actual penetration energy than that into the rod head. Therefore, the energy correction of the SPT N-value using the transferred energy into the sampler is more accurate than using that into the rod head. In addition, an instrumented dynamic cone penetrometer (IDCP) was developed to improve the DCP (Byun and Lee 2013). During the IDCP test, dynamic responses are obtained at the IDCP rod head and cone tip. The transferred energies into the rod head and cone tip are calculated using the dynamic responses. The estimation of soil resistance at the target ground is improved using transferred energies (Byun *et al*. 2014).

Portable devices such as light falling weight deflectometer (LFWD) are widely used to assess the stiffness of the ground (Kim *et al*. 2023). The LFWD measures the stiffness for a range of twice the loading plate diameter. A crosshole-type dynamic penetrometer (CDP), which is instrumented dynamic penetrometer based on the DCP, was developed to estimate the strength and stiffness of the ground, simultaneously (Hong *et al*. 2017). Signals of shear wave and penetration index are obtained during the CDP test. Shear wave velocity is calculated and used to estimate the shear modulus of ground. Hong *et al*. (2017) were measured the shear wave velocity in laboratory and field tests using bender elements and CDP, respectively. Measured shear wave velocities using bender elements and CDP were identical at the same depths.

This study introduces the smart instrumented dynamic penetrometers for soil resistance assessment. These penetrometers were developed to estimate the strength and stiffness of the ground and applied to field tests. The remainder of this study is organized as follows: Section 2 discusses the energy monitoring module for the SPT and introduces the background theory and experimental study using the energy monitoring module. Section 3 describes the design and field application of the IDCP incorporated with time domain reflectometry. Section 4 discusses the experimental procedure for shear wave velocity measurement using the CDP. Section 5 provides a summary and conclusions of the study.

2. Energy measurement in SPT

2.1 Energy monitoring module

The transferred energy into the rod head was measured using a typical energy monitoring module to correct the SPT N-value. Recently, the transferred energy into the sampler has been measured using the developed energy monitoring module to consider the rod effects and energy loss at joints (Lukiantchuki *et al*. 2011, Hong *et al*. 2022, Park *et al*. 2022). The energy measurement system in SPT using typical and developed energy monitoring modules is shown in Fig. 1. The typical and developed modules are located below the anvil and above the sampler, respectively. The accelerometer and strain gauges installed in the energy monitoring modules measure the signals of acceleration and force. The sensors in the typical module are outside, while those in the developed module are inside for protection. Measured signals using typical and developed modules are obtained by pile driving analyzer (PDA) and strain gauge bridge box, data logger, and computer, respectively. Input voltage and sampling rate of data logger are 1 V and 96 kHz, respectively.

2.2 Calculation of energy

The obtained signals of acceleration and force using

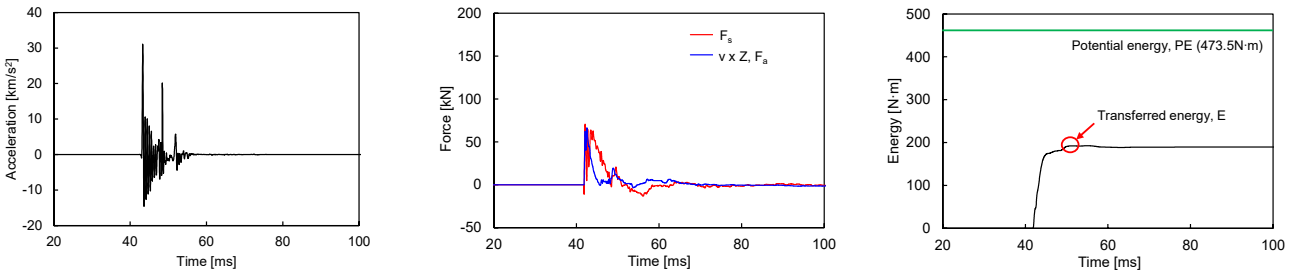

(a) Acceleration-time waveform (b) Force-time waveforms (c) Energy-time waveform

Fig. 2 Typical waveforms to calculate transferred energy

energy monitoring modules are employed to calculate the transferred energies into the rod head and sampler. The transferred energy (E) is calculated using time-varying functions of force (F_s) and velocity (v) based on ASTM D4633 (2005) as follows

$$E = max\left[\int F_s(t)v(t)dt\right] \quad (1)$$

F_s is measured by the strain gauges, and v is calculated by integrating the acceleration. The maximum value of integration at any time is determined to be E. Typical waveforms of acceleration, force, and E are represented in Fig. 2. Measured acceleration-time waveform is shown in Fig. 2(a). Fig. 2(b) shows the F_s and calculated force (F_a) by multiplying v by the impedance (Z). Calculated energy-time waveform I s represented in Fig. 2(c). The E is determined maximum value of energy-time waveform. Potential energy (PE = 473.5 N·m) is larger than determined E due to energy loss.

The calculated E and the theoretical PE are compared, while the ratio is defined as energy transfer ratio (ETR). In energy correction, the SPT N-value is corrected by a reference energy ratio of 60% using the ETR (Seed *et al.* 1985). The corrected SPT N-value is expressed as

$$N_{60} = \frac{ETR}{60} \cdot N = \frac{1}{60} \cdot \frac{E}{PE} \cdot N \quad (2)$$

The E is calculated from dynamic responses at either the rod head (E_{head}) or the sampler (E_{tip}).

Dynamic resistance (q_d) is calculated using the E and displacement (d) as follows

$$q_d = \frac{E}{d} = \frac{max[\int F_s(t)v(t)dt]}{d} \quad (3)$$

The q_t, which is result of the CPT, is similar with the q_d in coarse soils (Lee and Byun 2020). Penetration velocity of the SPT is 100 times larger than that of the CPT; thus, the q_d is larger than q_t due to the damping effects in fine soils (Lee and Byun 2020). In Eq. (3), the E_{head} and E_{tip} can be used to calculate q_d (q_{d_head} and $q_{d\_sampler}$).

2.3 Experimental study

The SPTs using the energy monitoring modules were conducted at the site. The CPTs were conducted near the borehole of SPT. The SPT N-value (N) and N_{60} based on the

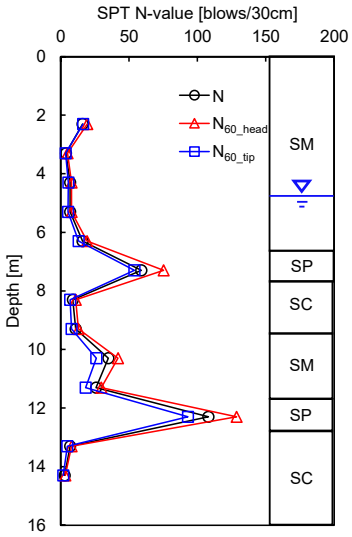

Fig. 3 Profile of SPT N-value (N) and corrected N_{60} by E_{head} and E_{tip} (N_{60_head} and N_{60_tip})

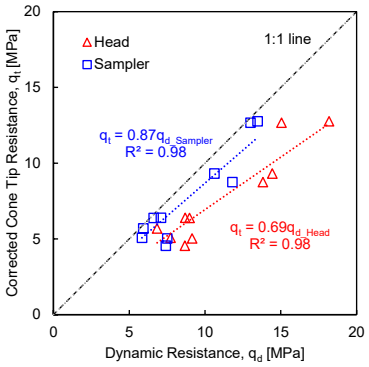

Fig. 4 Relationships between corrected cone tip resistance (q_t) and dynamic resistances (q_{d_head} and q_{d_tip})

E_{head} (N_{60_head}) and E_{tip} (N_{60_tip}) were plotted with the depth in Fig. 3. N_{60_tip} is larger than N_{60_head} due to the energy loss, as shown in Fig. 3. The soil types were also remarked according to the depth. The soils are classified as silty sand (SM) in most depths. At depths of 7.3 m and 12.3 m, the soils are classified as poorly graded sand (SP). The N-values at these depths are larger than other depths. The clayey sands are located at depths of 13.3 m and 14.3 m.

The q_t, q_{d_head} and q_{d_tip} are calculated according to the depth, as shown in Fig. 4. The q_t shows a similar tendency

with the q_{d_head} and q_{d_tip}. Resistances are determined to the soil types. Then, q_{d_head} and q_{d_tip} are plotted with the q_t as shown in Fig. 5. The determination coefficients of relationships are 0.98. The gradient of relationship between q_t and q_{d_tip} is 0.87, and it is larger than that between q_t and q_{d_head}. Therefore, the E_{tip} is more effectively used to calculate q_d than E_{head} because E_{tip} is more similar to the actual penetration energy.

3. Instrumented portable dynamic penetrometer

3.1 IDCP

The IDCP was designed to compensate for energy loss using a miniaturized energy monitoring module (Byun *et al.* 2015, Lee *et al.* 2019, Kim *et al.* 2021, Park *et al.* 2024). As shown in Fig. 5, the hammer with a weight of 117.7 N falls at a height of 575 mm to drive the rod during the IDCP test. The potential energy is calculated to be 67.7 N·m. The

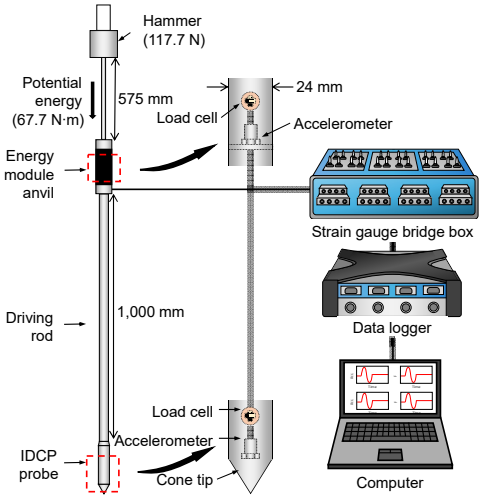

Fig. 5 Schematic drawing of instrumented dynamic cone penetrometer (IDCP)

nergy module anvil and IDCP probe are located at the rod head and cone tip. The accelerometers and strain gauges configured as full-bridge circuit are installed inside the energy module anvil and IDCP probe. An apex angle of the cone tip is 60°. The diameter of the cone tip, energy module, and IDCP probe is 24 mm. The strain gauge bridge box and data logger are used to obtain the dynamic responses. The dynamic responses at the rod head and cone tip are used to calculate the E and q_d based on Eqs. (1) and (3).

3.2 Incorporated with time domain reflectometry

Most slope failures are caused by heavy rainfall. During rainfall, rainwater infiltrates the ground on the slope. Consequently, the ground water level increases reducing ground strength (Likitlersuang *et al.* 2017). Thus, the characterization of strength and water content is crucial for evaluating slope stability. The IDCP may be effectively used to characterize the ground strength. The time domain reflectometry (TDR) method has been used to evaluate the dielectric constant and volumetric water content of soils. The dielectric constant is determined by impedance of material. Impedance of soils is significantly affected by water. Therefore, the dielectric constant is dependent on volumetric water content of soils. The pulse generated by TDR unit is transmitted the electrodes penetrate the soil, and the output voltages are changed. The variance of output voltages increases as the water content increases. The TDR probes have been developed in various forms. The TDR penetrometers were developed to estimate the dielectric constant and volumetric water content according to depth (Hong *et al.* 2019). The dielectric constants according to depth can be used to estimate the ground cavity with ground penetrating radar (Hong and Lee 2018).

Because property of two borehole is randomly distributed due to inhomogeneity of soils, tests using two penetrometers may be inaccurate. To characterize the ground strength and water content simultaneously, the IDCP incorporated with TDR (IDPT) was developed (Park *et al.*

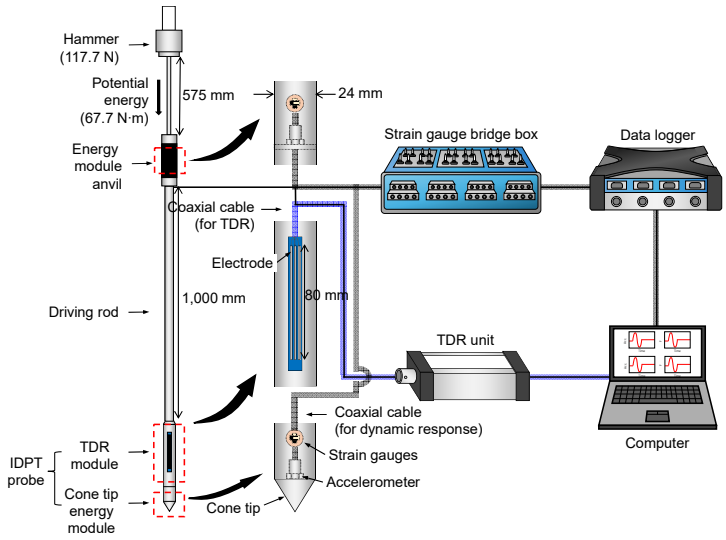

Fig. 6 Schematic drawing of instrumented dynamic cone penetrometer incorporated with time domain reflectometry

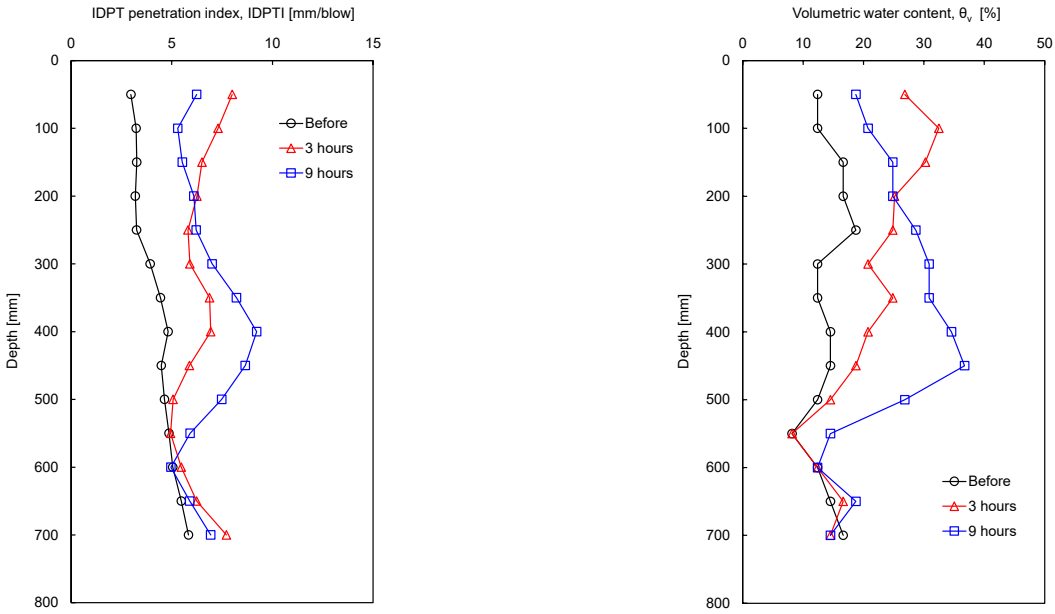

(a) IDPT penetration index (b) Volumetric water content

Fig. 7 IDPT test results according to depth before watering and after 3- and 9-hours watering

2023a). The IDCP is composed of a hammer, energy module anvil, driving rod, and IDPT probe as shown in Fig. 6. Specification of hammer, energy module anvil, and cone tip is identical with the IDCP. The IDPT probe is divided into TDR module and cone tip energy module. In TDR module, three electrodes with a length of 80 mm are installed in non-conducting material and connected to TDR unit.

3.3 Experimental study

The IDPT tests were conducted until a depth of 700 mm on compacted soils in an embankment. The embankment was compacted by 8 times using a 10-ton vibrating roller. Water of 90 mm per a unit area was sprayed onto the embankment to simulate the rainfall condition. The tests were performed before and after 3 and 9 h of watering. The IDPT penetration index (IDPTI) and volumetric water content were measured according to the depth as shown in Fig. 7. Fig. 7(a) shows the variation of ground strength according to the elapsed time for watering. Note that the IDPTI decreases as ground strength increases (Byun *et al.* 2013, Park *et al.* 2023b). After 3 h of watering, the IDPTI varies to a depth of 450 mm. The variation of the IDPTI is represented at a depth of 500 mm after 9 h of watering. The IDPTI after 3 h of watering is greatest at a depth of 150 mm. Next, the IDPTI increases with elapsed time. The profile of volumetric water content is shown in Fig. 7(b) according to the time. The volumetric water content after 3 h of watering is larger than that after 9 h of watering to a depth of 150 mm. For depths of 200 mm to 600 mm, the volumetric water content increases with elapsed time. The water infiltrates into the ground to a depth of 450 mm after 3 h of watering and a depth of 600 mm after 9 h of watering, respectively.

The IDPTI and volumetric water content at each depth

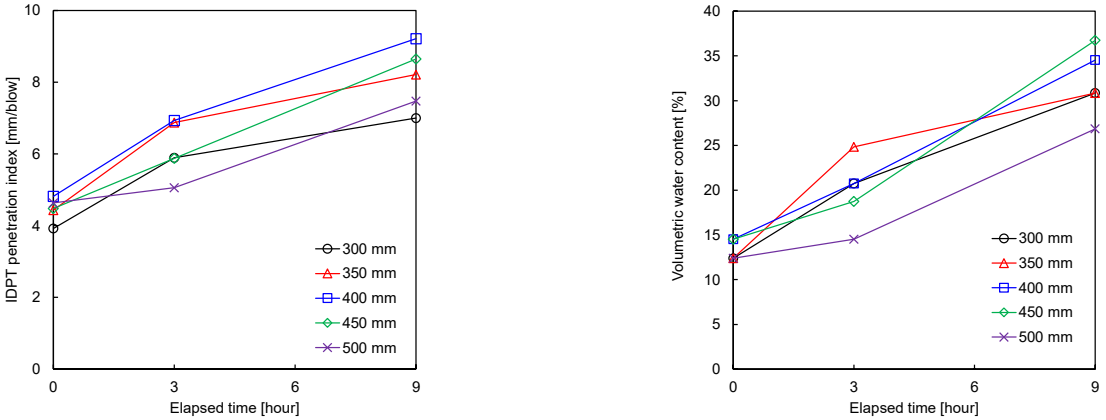

(c) IDPTI at depths of 250 mm - 500 mm (d) volumetric water content at depths of 250 mm - 500 mm

Fig. 8 Relationships between the IDPTI and volumetric water content and elapsed time

were plotted with the elapsed time, as shown in Fig. 8. Figs. 8(a) and 8(b) show the relationships between the IDPTI and volumetric water content and elapsed time at depths of 50 mm, 100 mm, and 150 mm, respectively. At a depth of 150 mm, the lowest strength and highest volumetric water content were measured after 3 h of watering due to the evaporation and infiltration of water. Thus, strength increases and volumetric water content decreases after 9 h of watering. The IDPTI and volumetric water content at depths of 250 mm to 550 mm were plotted with the elapsed time, as shown in Figs. 8(c) and 8(d). In these depths, as the volumetric water content increases with the elapsed time, the strength decreases. Therefore, water infiltration influences on strength and volumetric water content.

The IDPTI was plotted with the volumetric water content as shown in Fig. 9. Results at a depth of 50 mm were excluded due to the low density of soils near the surface. Low density causes inaccurate volumetric water content. In addition, data from depths greater than 500 mm, where water had not infiltrated, were excluded. The gradient and determination coefficient of the relationship between the IDPTI and volumetric water content are estimated to be 0.16 and 0.65, respectively. The IDPTI increases as the volumetric water content increases. Thus, the strength of the ground reduces with the volumetric water content. The infiltration of water reduces the strength of the ground and increase water content (Patel *et al*. 2013, Singh *et al*. 2017, Hussein and Alshkane 2018). Therefore, the IDPT may characterize the strength and water content of the ground, simultaneously.

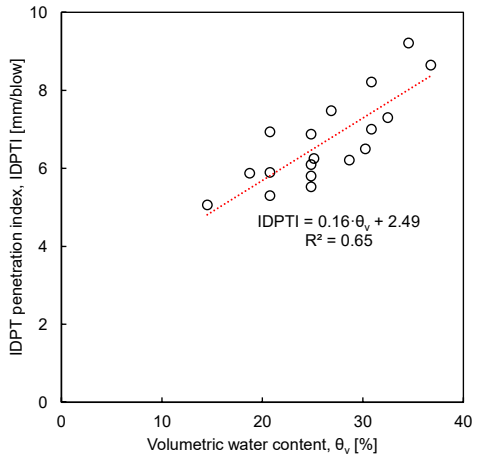

Fig. 9 Relationships between IDPT penetration index and volumetric water content

4. Shear wave velocity measured by dynamic penetrometer

4.1 CDP

Stiffness is a crucial parameter for the characterization of subsurface as strength. The crosshole-type dynamic penetrometer (CDP) was developed to estimate the strength and stiffness of the ground, simultaneously (Lee *et al*. 2021). The CDP is used to measure the CDP penetration index (CDPI) and shear wave velocity. The CDP consists of a hammer, an anvil, a driving rod, and the CDP probe, as shown in Fig. 10(a). Hammer weight and drop height are 117.7 N and 575 mm, respectively. Potential energy is fixed at 67.7 N·m. The probe cone tip diameter is 24 mm. An accelerometer with 10,000 g of capacity is installed in CDP probe to obtain acceleration signals, which are stored using a data logger and computer.

Fig. 10(b) shows the procedure of the CDP test. During the test, two CDPs, which are source- and receiver-CDP, were used. First, the receiver-CDP is penetrated into the ground by 100 mm. Next, the hammer drives the source-CDP, and the CDPI and acceleration signal are measured. The CDPI is calculated by the recorded penetration depths as follows

$$CDPI[mm/blow] = D_{n+1} - D_n \quad (4)$$

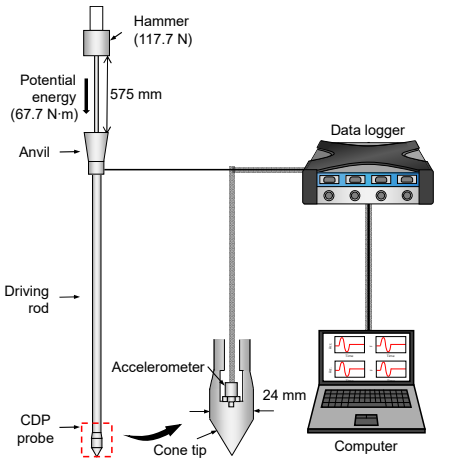

(a) Schematic drawing of CDP

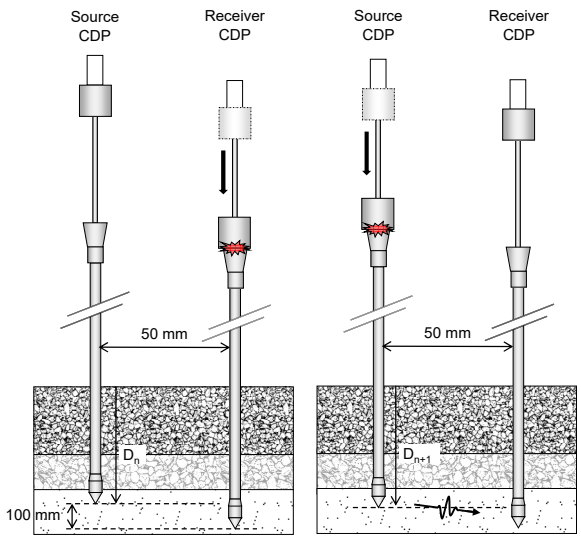

(b) CDP test procedure

Fig. 10 Crosshole-type dynamic penetrometer (CDP)

where D_{n+1} and D_n denotes the recorded penetration depths at $n+1^{th}$ and n^{th} blows, respectively. Profile of the CDPI indicates the variation of ground strength. The CDPI increases as the ground strength decreases.

4.2 Shear wave velocity

During the CDP test, the shear wave velocity can be calculated using the accelerometer per a blow. The shear wave velocity (V_s) is calculated using signals of acceleration at the source- and receiver-CDPs as follows

$$V_S[m/s] = \frac{L}{\Delta t} \tag{5}$$

where L is the distance between the source- and receiver-CDPs, and Δt is the travel time of shear wave. The travel time is the difference between first arrival times of shear waves measured using source- and receiver-CDPs. The first arrival time is peaked when acceleration changes.

To estimate the shear modulus of target ground, the V_s is employed as follows

$$G[MPa] = \rho \cdot {V_S}^2 \tag{6}$$

where G and ρ denote shear modulus and bulk density of the ground, respectively. The ρ depends on the material on target ground. The elastic modulus, which is a parameter of ground stiffness, is expressed using the G as

$$E[MPa] = 2(1+\nu)G \tag{7}$$

where ν is the Poisson's ratio. The Poisson's ratio is determined by soil types of the target ground.

4.3 Experimental study

The CDP tests were conducted on the roadbed in a mountainous ground to a depth of 800 mm. The ground of the roadbed is divided into three layers as: asphalt base (Layer 1), gravel sub-base (Layer 2), and sub-grade (Layer 3). Kim *et al*. (2024) obtained reflected shear waves in the roadbed, as shown in Fig. 11. Fig. 11 shows the signals of the source and receiver according to the penetration depth. However, as the depth increases, the first arrival time of the reflected shear wave decreases.

The first arrival times were marked, and the shear wave velocities were calculated using penetration depth and first arrival time. The calculated shear wave velocities were substituted into Eq. (6) to estimate the shear modulus. Bulk densities of asphalt base, gravel sub-base, and sub-grade are estimated to be 21.7 kN/m^3, 15.3 kN/m^3, and 15.3 kN/m^3, respectively, in accordance with the standard code of railway construction (Arosio 2016). Calculated shear modulus was used for evaluation of elastic modulus based on Eq. (7). The Poisson's ratio of asphalt base, gravel sub-base, and sub-grade are assumed to be 0.35, 0.40, and 0.45, respectively (Amakye *et al*. 2022).

Table 1 Comparison of estimated shear wave velocity

Layer	Shear wave velocity [m/s]			
	Nazarian (1984)	Hunaidi (1998)	Rosyidi *et al*. (2005)	Kim *et al*. (2024)
Asphalt base	2425	1000 -2500	900 - 2000	841-1202
Gravel sub-base	301.95	100 - 500	195 - 270	457-800
Sub-grade	271.45	80 - 300	200 - 400	147-202

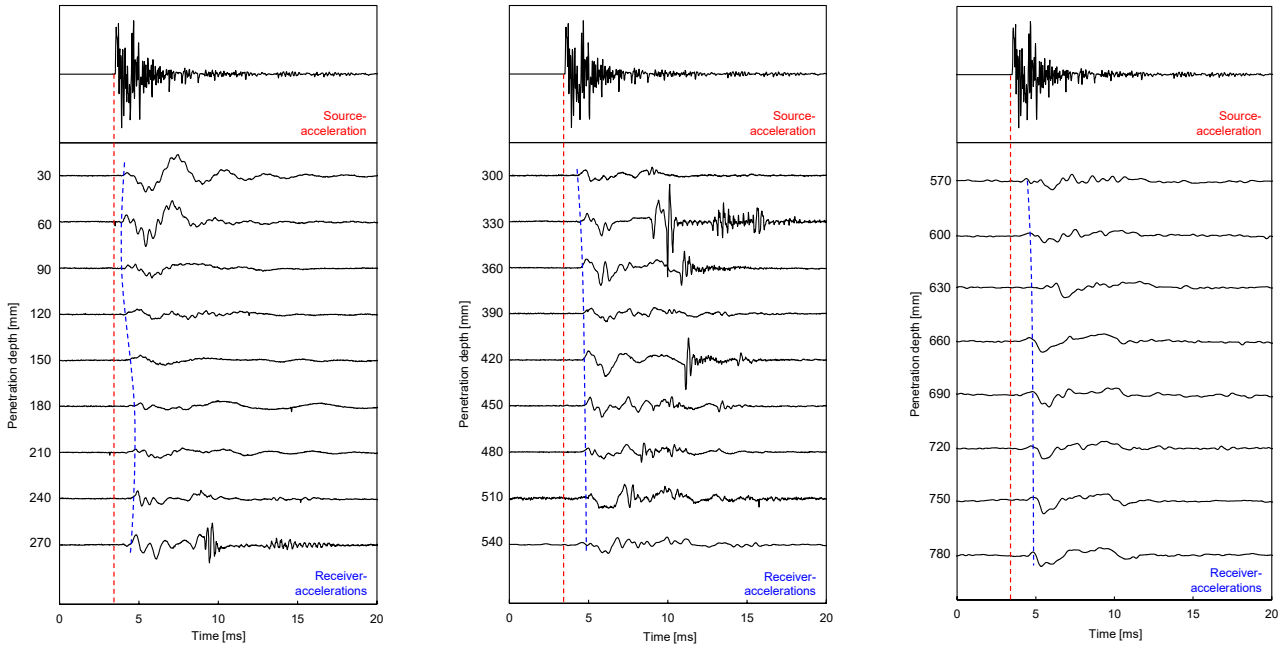

(a) Depth from 30 mm to 270 mm (b) Depth from 300 mm to 540 mm (c) Depth from 570 mm to 780 mm

Fig. 11 Shear waves obtained by source- and receiver-CDPs according to penetration depth (Kim *et al*. 2024)

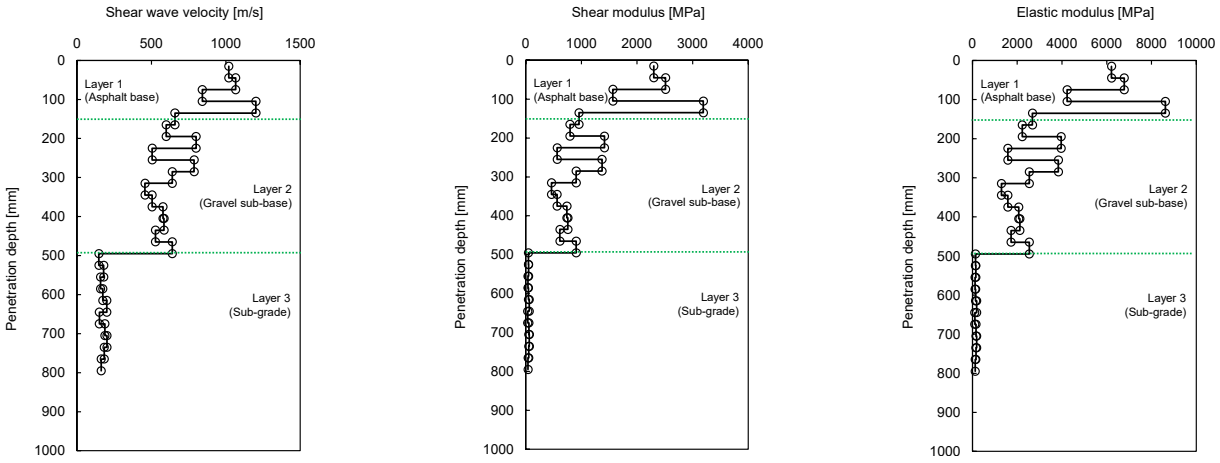

(a) Shear wave velocity (b) Shear modulus (c) Elastic modulus

Fig. 12 Profile of the ground stiffness parameters according to penetration depth (Kim *et al*. 2024)

Calculated shear wave velocity, shear modulus, and elastic modulus according to the penetration depth are represented in Fig. 12. Fig. 12(a) shows that the shear wave velocity decreases as the penetration depth increases. The ranges of the shear wave velocity are 841-1202 m/s in asphalt base, 457-800 m/s in gravel sub-base, and 147-202 m/s in sub-grade. In previous studies, the shear wave velocity in roadbed were estimated by surface wave method (Nazarian 1984, Hunaidi 1998, Rosyidi *et al*. 2005). Estimated shear wave velocities using the CDP tests are compared with those using the surface wave method in Table 1. Figs. 12(b) and 12(c) show profile of shear modulus and elastic modulus. Variations of shear modulus and elastic modulus characterize the stiffness of layers. The stiffness of ground is effectively estimated using the CDP.

5. Conclusions

In this study, smart instrumented dynamic penetrometers were introduced. Experimental studies using smart instrumented dynamic penetrometers were discussed to estimate the strength and stiffness of the ground. An energy monitoring module was developed to energy correct the standard penetration test (SPT) N-value. The dynamic response obtained by the energy module was used to calculate the dynamic resistances at the SPT rod head and sampler. The dynamic resistances were compared to corrected cone tip resistance measured by cone penetration test. Miniaturized dynamic penetrometer was instrumented using the energy monitoring module. Instrumented dynamic cone penetrometer (IDCP) was used to estimate the ground strength. Time domain reflectometry (TDR) is effective method to evaluate the volumetric water content. The IDCP incorporated with TDR (IDPT) was developed to characterize the ground strength and water content, simultaneously. The IDPT tests were applied on compacted soils in embankment under rainfall condition. The ground strength was correlated with the volumetric water content. Stiffness of ground was estimated using the crosshole-type penetrometer (CDP). Shear wave velocity of roadbed was profiled using the CDP. The main conclusions of this paper are summarized as follows:

- Transferred energy into the sampler is smaller than that into the rod head because of the energy loss. Dynamic resistance at the sampler is more similar to the corrected cone tip resistance than that at the rod head. The energy loss occurs at not only friction and anvil but also joints. Thus, the assessment of dynamic resistance at the sampler enhances the characterization of ground strength using SPT.
- IDCP is effectively used to characterize the ground strength in limited condition due to its high mobility. In addition, the water content of ground is simultaneously estimated with ground strength using the IDPT. In rainfall conditions, the ground strength and water content vary with time and depth. Characterization of the ground strength and water content according to the time and depth is crucial for estimating the stability of mountainous ground. Therefore, the IDPT is suitable for slope stability assessment.
- The CDP evaluates the strength and stiffness of the ground using the penetration index and shear wave velocity. Shear wave velocity of roadbed was measured using the CDP. The CDP test can replace the surface method, and the results of the CDP test had high resolution with depth. In addition, the ground strength can be simultaneously estimated using the CDP test. Accordingly, the CDP improves the profile of strength and stiffness for subsurface characterization. This study demonstrated that smart instrumented dynamic penetrometer can characterize the ground as an advanced in-situ testing device.

Acknowledgments

This work was supported by the National Research Foundation of Korea (NRF) grant funded by the Korea government (MSIT) (No. NRF-2021R1A5A1032433).

References

Amakye, S.Y., Abbey, S.J. and Booth, C.A. (2022), "Road pavement defect investigation using treated and untreated expansive road subgrade materials with varying plasticity index", *Transport. Eng.*, **9**, 100123. https://doi.org/10.1016/j.treng.2022.100123

Anbazhagan, P., Parihar, A. and Rashmi, H.N. (2012), "Review of correlations between SPT N and shear modulus: a new correlation applicable to any region", *Soil Dyn. Earthq. Eng.*, **36**, 52-69. https://doi.org/10.1016/j.soildyn.2012.01.005

Arifuzzaman and Anisuzzaman, M. (2022), "An initiative to correlate the SPT and CPT data for an alluvial deposit of Dhaka city", *Int. J. Geo-Eng.*, **13**(1), 5. https://doi.org/10.1186/s40703-021-00170-3

Arosio, D. (2016), "Rock fracture characterization with GPR by means of deterministic deconvolution", *J. Appl. Geophys.*, **126**, 27-34. https://doi.org/10.1016/j.jappgeo.2016.01.006

ASTM D4633 (2005), Standard test method for energy measurement for dynamic penetrometers; The American Society for Testing and Materials, West Conshohocken, USA.

ASTM D6951 (2009), Standard Test Method for Use f The Dynamic Cone Penetrometer in Shallow Pavement Applications; The American Society for Testing and Materials, West Conshohocken, USA.

Bolton Seed, H., Tokimatsu, K., Harder, L.F. and Chung, R.M. (1985), "Influence of SPT procedures in soil liquefaction resistance evaluations", *J. Geotech. Eng.*, **111**(12), 1425-1445. https://doi.org/10.1061/(ASCE)0733-9410(1985)111:12(1425)

Byun, Y.H. and Lee, J.S. (2013), "Instrumented dynamic cone penetrometer corrected with transferred energy into a cone tip: a laboratory study", *Geotech. Test. J.*, **36**(4), 533-542. https://doi.org/10.1520/GTJ20120115

Byun, Y.H., Kim, J.H. and Lee, J.S. (2013), "Cone penetrometer with a helical-type outer screw rod for evaluation of the subgrade condition", *J. Transport. Eng.*, **139**(2), 115-122. https://doi.org/10.1061/(ASCE)TE.1943-5436.00005

Byun, Y.H., Yoon, H.K., Kim, Y.S., Hong, S.S. and Lee, J.S. (2014), "Active layer characterization by instrumented dynamic cone penetrometer in Ny-Alesund, Svalbard", *Cold Regions Sci. Technol.*, **104**, 45-53. https://doi.org/10.1016/j.coldregions.2014.04.003

Byun, Y. H., Hong, W.T. and Lee, J.S. (2015), "Characterization of railway substructure using a hybrid cone penetrometer", *Smart Struct. Syst., Int. J.*, **15**(4), 1085-1101. http://dx.doi.org/10.12989/sss.2015.15.4.1085

Chang, M., Kuo, C.P., Shau, S.H. and Hsu, R.E. (2011), "Comparison of SPT-N-based analysis methods in evaluation of liquefaction potential during the 1999 Chi-chi earthquake in Taiwan", *Comput. Geotech.*, **38**(3), 393-406. https://doi.org/10.1016/j.compgeo.2011.01.003

Cubrinovski, M. and Ishihara, K. (1999), "Empirical correlation between SPT N-value and relative density for sandy soils", *Soils Found.*, **39**(5), 61-71. https://doi.org/10.3208/sandf.39.5 61

George, V., Nageshwar Rao, C. and Shivashankar, R. (2009), "Effect of soil parameters on dynamic cone penetration indices of laterite sub-grade soils from India", *Geotech. Geolog. Eng.*, **27**, 585-593. https://doi.org/10.1007/s10706-008-9248-6

Hong, W.T. and Lee, J.S. (2018), "Estimation of the Ground Cavity Configurations using Ground Penetrating Radar and Time Domain Reflectometry", *Natural Hazards*, **92**(3), 1789-1807. https://doi.org/10.1007/s11069-018-3278-z

Hong, W.T., Kim, S.Y., Lee, S.J. and Lee, J.S. (2017), "Strength and stiffness assessment of railway track substructures using crosshole-type dynamic cone penetrometer", *Soil Dyn. Earthq. Eng.*, **100**, 88-97. https://doi.org/10.1016/j.soildyn.2017.05.021

Hong, W.T., Yu, J.D., Kim, S.Y. and Lee, J.S. (2019), "Dynamic cone penetrometer incorporated with time domain reflectometry (TDR) sensors for the evaluation of water contents in sandy soils", *Sensors*, **19**(18), 3841. https://doi.org/10.3390/s19183841

Hong, W.T., Kim, S.Y. and Lee, J.S. (2022), "Evaluation of driving energy transferred to split spoon sampler for accuracy improvement of standard penetration test", *Measurement*, **188**, 110384. https://doi.org/10.1016/j.measurement.2021.110384

Hunaidi, O. (1998), "Evolution-based genetic algorithms for analysis of non-destructive surface wave tests on pavements", *NDT & e Int.*, **31**(4), 273-280. https://doi.org/10.1016/S0963-8695(98)00007-3

Hussein, A.A. and Alshkane, Y.M. (2018), "Prediction of CBR and MR of fine-grained soil using DCPI", *Proceedings of the 4th International Engineering Conference on Developments in Civil & Computer Engineering*, pp. 268-282.

Ji, Y., Kim, B. and Kim, K. (2021), "Evaluation of liquefaction potentials based on shear wave velocities in Pohang City, South Korea", *Int. J. Geo-Eng.*, **12**, 1-10. https://doi.org/10.1186/s40703-020-00132-1

Kim, S.Y., Lee, J.S., Kim, D.J. and Byun, Y.H. (2021), "Comparative study on estimation methods of dynamic resistance using dynamic cone penetrometer", *Sensors*, **21**(9), 3085. https://doi.org/10.3390/s21093085

Kim, S.Y., Lee, J.S., Tutumluer, E. and Byun, Y.H. (2022), "Dynamic response of free-end rod with consideration of wave frequency", *Geomech. Eng., Int. J.*, **28**(1), 25-33. https://doi.org/10.12989/gae.2022.28.1.025

Kim, N., Lee, J.S., Park, G., Kang, S., Han, W. and Hong, W.T. (2023), "Strength and stiffness characterizations of geo-materials composing unpaved roads using LFWD, DCP, and CDP tests", *Constr. Build. Mater.*, **402**, 132592. https://doi.org/10.1016/j.conbuildmat.2023.132592

Kim, S.Y., Kang, S., Park, G., Lee, D., Lim, Y. and Lee, J.S. (2024), "Detection of roadbed layers in mountainous area using down-up-crosshole penetrometer and ground penetrating radar", *Measurement*, **224**, 113889. https://doi.org/10.1016/j.measurement.2023.113889

Kovacs, W.D. (1979), "Velocity measurement of free-fall SPT hammer", *J. Geotech. Eng. Div.*, **105**(1), 1-10. https://doi.org/10.1061/AJGEB6.0000748

Kumar, R., Bhargava, K. and Choudhury, D. (2016), "Estimation of engineering properties of soils from field SPT using random number generation", *INAE Letters*, **1**, 77-84. https://doi.org/10.1007/s41403-016-0012-6

Lee, J.S. and Byun, Y.H. (2020), "Instrumented cone penetrometer for dense layer characterization", *Sensors*, **20**(20), 5782. https://doi.org/10.3390/s20205782

Lee, J.S., Kim, S.Y., Hong, W.T. and Byun, Y.H. (2019), "Assessing subgrade strength using an instrumented dynamic cone penetrometer", *Soils Found.*, **59**(4), 930-941. https://doi.org/10.1016/j.sandf.2019.03.005

Lee, J.S., Tutumluer, E. and Hong, W.T. (2021), "Stiffness evaluation of compacted geo-materials using crosshole-type dynamic cone penetrometer (CDP), rPLT, and LFWD", *Constr. Build. Mater.*, **303**, 124015. https://doi.org/10.1016/j.conbuildmat.2021.124015

Likitlersuang, S., Takahashi, A. and Eab, K.H. (2017), "Modeling of root-reinforced soil slope under rainfall condition", *Eng. J.*, **21**(3), 123-132. https://doi.org/10.4186/ej.2017.21.3.123

Lukiantchuki, J.A., Esquivel, E.R. and Bernardes, G.D.P. (2011), "Interpretation of force and acceleration signals during hammer impact in SPT tests", *Proceedings of 14th Pan-American Conference on Soil Mechanics and Geotechnical Engineering*, Toronto, Canada.

Mohammadi, S.D., Nikoudel, M.R., Rahimi, H. and Khamehchiyan, M. (2008), "Application of the Dynamic Cone

Penetrometer (DCP) for determination of the engineering parameters of sandy soils", *Eng. Geol*., **101**(3-4), 195-203. https://doi.org/10.1016/j.enggeo.2008.05.006

Mujtaba, H., Farooq, K., Sivakugan, N. and Das, B.M. (2018), "Evaluation of relative density and friction angle based on SPT-N values", *KSCE J. Civil Eng*., **22**, 572-581. https://doi.org/10.1007/s12205-017-1899-5

Nazarian, S. (1984), "In situ shear wave velocities from spectral analysis of surface wave", *Proceedings of 8th Conference on Earthquake Engineering*, San Francisco, CA, USA.

Park, G., Kim, N., Hong, W.T. and Lee, J.S. (2022), "Rod effects on transferred energy into SPT sampler using smart measurement system", *Smart Struct. Syst*., *Int. J*., **30**(2), 159-172. https://doi.org/10.12989/sss.2022.30.2.159

Park, G., Kim, N., Kang, S., Kim, S.Y., Yoo, C. and Lee, J.S. (2023a), "Instrumented dynamic cone penetrometer incorporated with time domain reflectometry", *Measurement*, **206**, 112337. https://doi.org/10.1016/j.measurement.2022.112337

Park, G., Lee, J.S., Kim, N., Lee, D. and Kim, S.Y. (2023b), "Effects of weight and drop height of hammer on dynamic cone penetration test in loose layer", *Measurement*, **218**, 113198. https://doi.org/10.1016/j.measurement.2023.113198

Park, G., Lee, J.S., Kim, N. and Kim, S.Y. (2024), "Hammer weight and dropping height effects on dynamic response in densely packed geo-materials", *Transport. Geotech*., **44**, 101170. https://doi.org/10.1016/j.trgeo.2023.101170

Patel, M.A., Patel, H.S. and Dadhich, G. (2013), "Prediction of subgrade strength parameters from dynamic cone penetrometer index, modified liquid limit and moisture content", *Procedia-Social Behav. Sci*., **104**, 245-254. https://doi.org/10.1016/j.sbspro.2013.11.117

Rosyidi, S.A.P., Ismail, M.A., Samsudin, A.R., Taha, M.R., Rafek, A.G. and Nayan, K.A.M. (2005), "In Situ Determination of Layer Thickness And Elastic Moduli Of Asphalt Pavement Systems By Spectral Analysis Of Surface Waves (Sasw) Method", *Semesta Teknika*, **8**(2), 159-171. https://doi.org/10.18196/st.v8i2.904

Sagar, C.P., Badiger, M., Mamatha, K.H. and Dinesh, S.V. (2022), "Prediction of CBR using dynamic cone penetrometer index", *Materials Today*: *Proceedings*, **60**, 223-228. https://doi.org/10.1016/j.matpr.2021.12.467

Sakib, S., Islam, M.A. and Hossain, M.S. (2022), "Assessment of the Seasonal and Spatial Variation in Shear Strength of High Plasticity Clay on Highway Slopes Using DCP Tests", In: *Geo-Congress 2022*, pp. 524-533. https://doi.org/10.1061/9780784484036.05

Scala, A.J. (1956), "Simple methods of flexible pavement design using cone penetrometers", *New Zealand Eng*., **11**(2), 34-44.

Seed, B.H., Tokimatsu, K., Harder, L.F. and Chung, R.M. (1985), "Influence of SPT procedures in soil liquefaction resistance evaluations", *J. Geotech. Eng*., **111**(12), 1425-1445. https://doi.org/10.1061/(ASCE)0733-9410(1985)111:12(1425)

Singh, D., Jha, J.N. and Gill, K.S. (2017), "Effect of field moisture content on penetration index value of dynamic cone penetrometer in alluvial soil subgrades", *Int. J. Eng. Sci. Res. Technol*., **6**(7), 327-333.

Sjoblom, D., Bischoff, J. and Cox, K. (2002), "SPT Energy Measurements with the PDA", *Proceedings of the 2nd International Conference on the Application of Geophysicals and NDT Methodologies to Transportation Facilities and Infrastructure*, Los Angeles, CA, USA, April.

Tsuchida, T., Athapaththu, A.M.R.G., Kano, S. and Suga, K. (2011), "Estimation of in-situ shear strength parameters of weathered granitic (Masado) slopes using lightweight dynamic cone penetrometer", *Soils Found*., **51**(3), 497-512. https://doi.org/10.3208/sandf.51.497